https://doi.org/10.46813/2024-150-048

UDC 546.3-19'11

APPLICATION OF HIGH-ENTROPY ALLOYS IN HYDROGEN STORAGE TECHNOLOGY

Sergiy Karpov
National Science Center "Kharkov Institute of Physics and Technology", Kharkiv, Ukraine
E-mail: karpofff@kipt.kharkov.ua

High-entropy alloys (HEAs), a new class of materials with promising structural and functional properties, have recently garnered significant attention in various fields, including hydrogen storage. Their unique design concept and vast compositional diversity offer unprecedented opportunities for the development of advanced hydrogen storage materials. This review aims to systematically analyze the current research status of high-entropy alloys for hydrogen storage, with a focus on compositional designs, synthesis processes, and hydrogen storage characteristics. The review also examines correlations between hydrogen storage performance and composition-related properties, particularly for hydrogen storage alloys crystallizing as BCC solid solutions and Laves phase structures. Various aspects of hydrogen interaction with HEAs, including reversibility of hydrogen storage, cycling stability, and activation behavior have been considered in detail. The potential of HEAs in the development of novel hydrogen storage materials with superior performance is highlighted, emphasizing the importance of effective compositional design and synthesis methods.

INTRODUCTION

Hydrogen is considered to be the cleanest fuel with the potential to replace fossil fuels. However, its storage is a major challenge. Conventionally, hydrogen storage in gaseous and liquid form has been employed for various applications, but none of them can provide storage in a safe and efficient manner. Gaseous hydrogen storage systems require a very high-pressure compressed gas tank which is quite unsafe and the storage in the liquid form needs cryogenic vessels maintaining the temperature about 20 K. Furthermore, these approaches have limitations in terms of both volumetric and gravimetric storage densities [1]. As widely adopted criterion for assessment, the US Department of Energy (DOE) has established requirements for gravimetric and volumetric density in on-board hydrogen storage systems. These targets are defined as 0.045 kg (H_2)/kg (storage system) (equivalent to 4.5 wt.%) for gravimetric density and a volumetric capacity of 0.030 kg·L^{-1} (0.030 g·cm^{-3}). The specified storage conditions include temperatures ranging from –40 to +60 °C and pressures between 5…12 bar [2]. At present, neither the gaseous nor liquid forms of hydrogen storage meet the DOE targets.

As alternative to current tank-based storage methods the materials based storage in the form of metal hydrides provides the most compact and effective technology (Fig. 1). Hydrogen can be stored in solid materials with higher concentration of hydrogen compared to the gaseous and liquid hydrogen storage systems. Moreover, hydrogen storage as a form of metal hydride is the safest storage mode to use hydrogen for stationary and mobile applications.

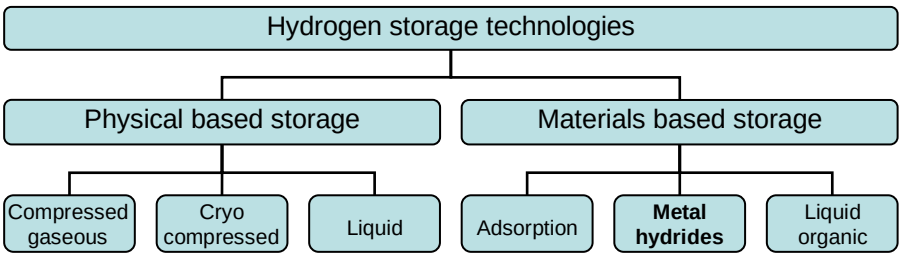

Fig. 1. Hydrogen storage technologies

For most of the practical applications of hydrogen storage materials, they should have several features such as the ability for reversible absorption and desorption of hydrogen at ambient temperature, fast absorption/desorption rate, feasible hydrogen absorption/desorption pressure and high cycling stability.

Various solid hydrogen storage materials, including complex hydrides, Mg-based metal hydrides, and intermetallic hydrides, have been studied for practical applications [3–8]. However, none of these materials meets all the requirements for competitive hydrogen storage. Magnesium hydride and complex hydrides, known for their high storage capacity, are limited by their high thermodynamic stability, restricting their use to high temperatures. While some materials like TiFe and $LaNi_5$ have been suggested for room-temperature hydrogen storage, they face challenges such as activation issues in TiFe and low storage capacity in $LaNi_5$ [9–11]. In addition, commonly used metals are expensive and heavy for mobile applications, and their constituent elements (e.g. La, Pd) are often scarce. Consequently, there is a significant demand for new metal hydride systems that can meet the requirements for hydrogen storage at ambient temperature.

In this regard, a new class of alloys, namely, high-entropy alloys, which are solid solutions of five or more principal elements in nearly equal quantities, have received significant attention for hydrogen storage applications. The variety of compositional configurations that may be obtained by selection of principal elements and their concentrations offers many options for modifying the properties of hydrides [12]. It may provide new possibilities in the development of solid-state hydrogen storage.

The concept of HEAs was introduced independently by Cantor et al. [13] and Yeh et al. [14] in 2004. It was subsequently found that essential technological properties of HEAs are associated with four core effects: the high-entropy effect, sluggish diffusion effect, severe lattice distortion effect, and cocktail effect [15–17], which may play a crucial role in achieving prospective hydrogen storage systems. The high-entropy effect promotes the formation of solid solution phases such as face-centered cubic (FCC) or body-centered cubic (BCC), creating a substantial void space for hydrogen. The sluggish diffusion effect facilitates the formation of nano-grains, which enhances the hydrogen absorption and desorption kinetics. The severe lattice distortion effect is related to the difference in atomic radius resulting in large interstitial sites, which are beneficial to the hydrogen storage properties [18, 19]. The cocktail effect is a concept based on the synergy of the other three effects, which influences the physical and chemical properties of HEAs.

The behavior of multicomponent systems is complicated due to the interplay of elemental components with diverse properties such as valence, electronegativity, hydrogenation ability, atomic size, melting temperature, and density. In multicomponent systems forming solid solutions, mixing entropy values increase with the number of components. A comprehensive understanding of ordering behaviors in these systems is crucial. To assess ordering behaviors effectively, various aspects of metal-hydrogen interactions must be considered, including mechanisms of hydrogen interaction with HEAs, site occupancies by hydrogen atoms in interstitial sites, reversibility of hydrogen storage performance, cycle stability, and activation behaviors. Both experimental and theoretical studies contribute to deepening the fundamental knowledge of metal-hydrogen systems, facilitating the explanation of HEAs performance as hydrogen storage materials. This understanding is particularly related to the diversity of interstitial sites characterized by different chemical environments linked to the types and numbers of constituent elements. Meanwhile, studies aimed at understanding the operating mechanisms that determine the efficiency of hydrogen storage are a high priority.

Due to the aforementioned features of HEAs, extensive efforts have been devoted to the design and investigation of hydrogen storage properties in high-entropy alloys. Since the first publication by Kao et al. [20] focusing on hydrogen storage in $CoFeMnTi_xV_yZr_z$ HEAs in 2010, numerous subsequent studies have been carried out, resulting in some promising findings. Recently, there has been an increasing interest in this research area, which has led to a marked increase in the number of papers published each year.

Hydrogen storage capacity is an important parameter for practical applications and has been the subject of recent investigations. Notably, the HEAs of Ti–V–Nb–Cr-system have achieved a remarkable maximum hydrogen storage capacity of 3.7 wt.% [21, 22]. These specific findings have contributed significantly to understanding the design criteria for HEAs in hydrogen storage. Various approaches such as empirical models, first-principles calculations, and machine learning algorithms have been considered in recent studies, shaping the current research landscape and providing insights into future directions.

This paper aims to consolidate the recent advancements in hydrogen-storage HEAs. The review examines preparation methods, theoretical predictions, alloy types, and hydrogen-storage performance. The main contents are organized as follows: first, the basics of hydrogen interaction with metals are outlined. Then, the design of HEAs for hydrogen storage, including theory, calculations, and synthesis processes, is discussed. The following section provides a detailed analysis of the hydrogen storage properties of HEAs with BCC and Laves phase structures, including capacity, hydrogenation kinetics, and cycling behavior. Finally, concluding remarks are made in Summary section.

1. BASICS OF HYDROGEN INTERACTION WITH METALS

Molecular hydrogen from the gas phase can be used to form metal hydrides. The process of hydrogen reacting with metal occurs in several stages. Initially, the hydrogen molecule interacts with the metal surface through the Van der Waals force, resulting in a physically adsorbed state. This interaction involves a gas molecule interacting with multiple atoms on the solid surface. The interaction is characterized by an attractive term, which decreases as the distance between the hydrogen molecule and the solid metal increases. The molecule's potential energy has a minimum at approximately one molecular radius. In the next stage of the hydrogen-metal interaction, the hydrogen has to overcome an activation barrier for dissociation and formation of the hydrogen-metal bond. This process is known as dissociation and chemisorption. The chemisorption energy is significantly higher than the respective energy for physical adsorption. Following dissociation on the metal surface, the hydrogen atoms diffuse into the bulk to form a Me-H solid solution. Fig. 2 shows schematic representation of described process of hydrogen interaction with metals.

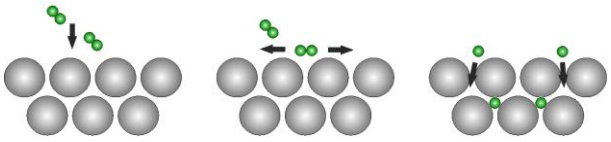

Fig. 2. Schematic representation of hydrogen absorption process from the gas phase

In conventional metals, hydrogen occupies interstitial sites, either tetrahedral or octahedral, in the

metal host lattice. When the hydrogen concentration in the host metal exceeds a certain value (usually H/Me > 0.1), a strong interaction between hydrogen atoms becomes significant due to lattice expansion. Chemical bonds form between hydrogen and metal atoms, leading to the nucleation and growth of the hydride phase. Fig. 3 shows simplified one-dimensional potential energy curves of hydrogen in molecular and atomic form interacting with a metal.

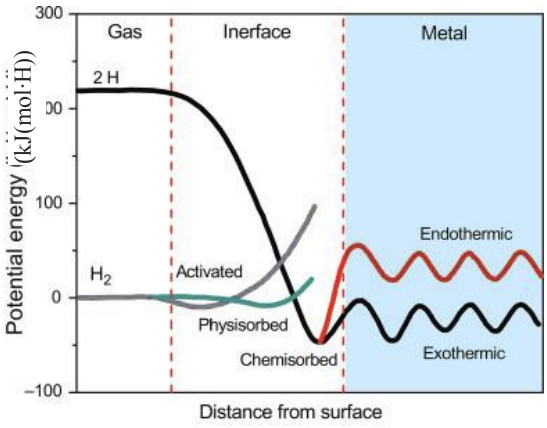

Fig. 3. Schematic of potential energy curves of hydrogen-metal interaction (according to [23])

The description of the thermodynamic aspects associated with the formation of hydrides from gaseous hydrogen is revealed through pressure-composition isotherms, as illustrated in Fig. 4. When both solid solution (commonly referred to as the α-phase) and hydride phase (β-phase) are present, a plateau appears in the isotherms, which determines the amount of stored hydrogen. The temperature-dependent plateau pressure within this two-phase region represents also the equilibrium dissociation pressure of the hydride and serves as an indicator of the stability of the hydride. Following the complete transformation to the hydride phase, additional hydrogen dissolution occurs simultaneously with an increase in pressure.

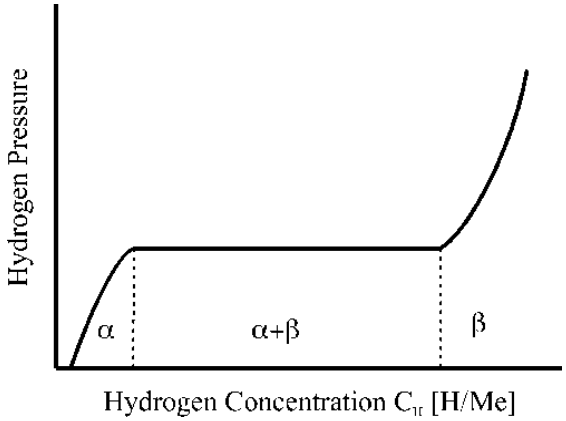

Fig. 4. Schematic pressure-composition isotherm

The absorption/desorption of hydrogen in potential hydrogen storage materials occurs through a solid-gas reaction with multiple energy barriers (see Fig. 3). This stage is an interface-controlled reaction. The second stage involves the permeation of hydrogen atoms into the material bulk, which is a diffusion-controlled reaction limited by the diffusion coefficient in certain alloys. The metal hydride formation/decomposition is the third key stage of Me-H interaction, which is characterized by hydrogen binding energy. To realize the application of metal hydrides for hydrogen storage, they should have the capability for reversible uptake and release of hydrogen at appropriate temperatures. Therefore, each of the above stages is of critical importance and should be carefully controlled when designing HEAs for hydrogen storage.

Some hydrogen absorption alloys have limited capacity for hydrogen absorption upon their first exposure to hydrogen [24]. However, after undergoing activation, characterized by a number of hydrogen absorption/desorption cycles, they obtain the ability to readily absorb hydrogen. The activation of a metal hydride during its initial hydrogenation is a gradual process that typically requires elevated temperature and pressure.

The activation mechanism has been extensively studied and its sensitivity to the surface state of the hydrogen absorption alloys has been demonstrated. The surfaces of most hydrogen absorption alloys are susceptible to contamination by the formation of oxides when exposed to the air. The primary obstacle to hydrogen absorption is the resulting surface oxide layer. This layer impedes the dissociation of hydrogen molecules into atoms and the permeation of hydrogen atoms into the bulk material [25]. For instance, the effect of oxide film on the deuterium permeation behavior in CoCrMnFeNi high-entropy alloy after oxidation at 823 K for 24 h was studied in [26]. The results show that an oxide film with a thickness of about 1 μm was formed on the surface of the sample after oxidation. The outer layer of the oxide film is rich in Mn_2O_3 and the inner layer is rich in Cr_2O_3. The deuterium permeability of the CoCrMnFeNi sample after oxidation was reduced by an order of magnitude compared to that for the unoxidized one.

Several hypotheses have been proposed to explain the activation process, including the dissociation of surface oxides into metals or suboxides [27], the transformation of oxides into suboxides and sub-hydroxides [24], the creation of cracks in the surface oxide layer to expose fresh metallic surfaces to hydrogen [28], and the initiation of new phases at the surface [29, 30]. Addressing the issue of activation is critical to the improvement of the performance of hydrogen absorbing alloys.

Hydrogen permeation behaviors can vary significantly in different HEAs, as demonstrated, for example, by the results of recent study [31]. This study compares the permeability of AlCoCrFeNi (BCC) and CoCrMnFeNi (FCC) and attributes the differences to variations in diffusion coefficients and deuterium solubility in these HEAs. The diffusion coefficients were obtained from the lag time in the permeation experiments, and it was found that the deuterium diffusion coefficient in AlCoCrFeNi is higher than that in CoCrMnFeNi. The solubility of deuterium in AlCoCrFeNi is lower than that in CoCrMnFeNi. The differences in crystal structures, and element types of these HEAs may contribute to the observed variations in behavior. The authors also emphasized that the

microscopic structure (e.g., the size, distribution, and orientation of the crystal grains), dislocations, and sample state of these HEAs may contribute to the different behavior of deuterium diffusion and solubility.

The hydrogen binding energy is the most important parameter that requires adjustment for reversible hydrogen storage at room temperature. The dehydrogenation temperature increases and the equilibrium hydrogen pressure decreases as the absolute value of the negative binding energy increases. However, materials that exhibit appropriate hydrogen binding energies for room-temperature hydrogen storage are limited. The goal is to adjust the elemental composition of potential high-entropy alloys to achieve a hydrogen binding energy that is slightly more negative than -0.1 eV [32, 33].

Studies focusing on the kinetics of specific stages of hydrogen-surface/matrix interactions in hydrogen storage alloys are quite rare, and new data would be very useful for developing more efficient design strategies for high-entropy alloys. Additional effects of hydrogen permeation in the material bulk may arise due to the influence of interfaces of the particles that compose the alloy. These interfaces can either accelerate or inhibit hydrogen permeation. The formation of interfaces, as well as the size of the particles, depends on the method of preparation of HEAs, which will be discussed in the next section.

2. SYNTHESIS PROCESSES

All existing methods of preparing high-entropy alloys have a variety of competing features that can contribute to the optimization of hydrogen storage properties. Each specific technique affects the homogeneity of the material, its microstructure, crystal structure, and defect formation, consequently influencing the hydrogen storage behavior. Careful consideration of each component is important when selecting the most appropriate method for material development.

In hydrogen storage alloys, the primary component is a hydride-forming element A, which readily interacts with hydrogen, resulting in the formation of a stable hydride accompanied by a considerable release of heat ($\Delta H < 0$). This component plays a crucial role in regulating the quantity of hydrogen stored in the alloy. Titanium (Ti), and zirconium (Zr) emerge as the most frequently utilized hydride-forming elements, contributing to almost all known HEA alloys. The second component is a non-hydride-forming element B, which typically does not react with hydrogen and has minimal affinity for it. However, when hydrogen dissolves in this metal, it absorbs heat ($\Delta H > 0$), thereby influencing the reversibility of hydrogen absorption and release [12, 34]. Among elements that do not form stable hydrides, chromium (Cr), manganese (Mn), and iron (Fe) are found most frequently in the compositions of known HEAs. The enthalpy of hydride formation in HEA alloys can be adjusted by combining elements with different enthalpies of hydride formation.

In terms of binding energies, A-type elements exhibit negative hydrogen binding energies, leading to the formation of stable hydrides, while B-type elements possess positive binding energies and generally do not absorb hydrogen. Consequently, the combination of A-type and B-type elements can facilitate the formation of alloys with appropriately low hydrogen binding energies for room-temperature hydrogen storage [33].

The HEA synthesis techniques can be classified into four ways: liquid state, solid state, gaseous state, and electrochemical preparation techniques [35]. The liquid-state synthesis techniques include arc melting, resistance melting, induction melting, laser melting, laser cladding, and laser-engineered net shaping (LENS) [36, 37]. The main methods of solid-state synthesis are mechanical alloying and spark plasma sintering (SPS) [38]. Atomic layer deposition (ALD), molecular beam epitaxy (MBE), and vapor-phase deposition are gas-phase methods. A recent review article by Wang et al. [39] summarizes various methods of HEA synthesis and their advantages.

HEAs explored for hydrogen storage are mostly synthesized either by arc melting or by high energy ball-milling, which are particularly suitable for small series or experimental applications.

According to existing literature, the most commonly used method for preparing hydrogen storage HEAs is arc melting, which can be performed under vacuum or inert atmosphere [40–49]. This process involves melting high-purity elemental metals up to their melting point and rapidly cooling them to room temperature, resulting in a material with minimal contamination and reduced structural defects. One potential limitation of the technique is the formation of a non-equilibrium structure [50], which may restrict the material's capacity for hydrogen storage. It may be necessary to remelt the material several times to achieve an equilibrium structure and ensure homogeneity. In the context of hydrogen storage materials, particular attention should also be devoted to controlling the cooling rate after melting. Slow cooling leads to larger grains, potentially diminishing hydrogen diffusion rates throughout the material. Conversely, rapid solidification generally results in finer microstructures, enhancing the kinetics of hydrogen exchange during the formation-decomposition of hydrides [51].

The second most preferred approach for synthesizing HEAs is ball milling (BM). This method involves multiple cycles of extrusion, cold welding, fracture, and re-extrusion of the mixture, along with high-velocity collisions between the alloy powder and grinding balls in a high-energy ball mill [52]. The refinement of particle size and alloying processes in this procedure is influenced by milling parameters such as ball-to-powder weight ratio (BPR), ball size, rotation speed, milling time, process control agent (PCA), and type of milling media [53, 54]. Notably, this technique yields a more homogeneous sample composition compared to the arc-melting approach and operates at lower temperatures. Numerous studies [55–61] have explored the mechanical alloying process for fabricating hydrogen-storage HEAs, especially those containing light elements (Mg and Al), which are unsuitable for arc melting due to their high equilibrium vapor pressures and low melting temperatures.

3. DESIGN OF HEAS FOR HYDROGEN STORAGE: THEORY AND CALCULATIONS

Thermodynamic-based design strategies have become essential tools for predicting phase formation and stability in diverse HEA systems due to the extensive array of potential compositions and their unexplored properties. Various computational techniques are commonly used to facilitate the discovery of novel HEA compositions. These methods include empirical models, first-principles calculations, Calculation of Phase Diagrams (CALPHAD), and machine learning algorithms.

Empirical models provide a practical solution in the absence of reliable phase diagrams or access to high-performance computing resources. Furthermore, unknown composition can be predicted based on calculations using the Hume-Rothery rules, as the necessary thermophysical parameters can be easily obtained [62]. In the empirical methodology, expressions for atomic size mismatch (δ), electronegativity ($\delta\chi$), and valence electron concentration (VEC), along with several thermodynamic factors such as mixing entropy/enthalpy ($\Delta H_{\text{mix}}/\Delta S_{\text{mix}}$), are determined from the alloy's composition. The parameters δ, $\delta\chi$, VEC, ΔH_{mix}, and ΔS_{mix} are defined as follows:

$$\delta = \sqrt{\sum c_i \left(1 - \frac{r_i}{\bar{r}}\right)^2} \times 100 , \quad (1)$$

where c_i is the atomic percentage of the i-th component; r_i is the atomic radius of the i-th element, and $\hat{r}$ is the average atomic radius.

$$\delta_\chi = \sqrt{\sum c_i \left(1 - \frac{\chi_i}{\bar{\chi}}\right)^2} \times 100 , \quad (2)$$

where χ_i is the electronegativity of element i; χ is the average of the electronegativity.

$$\text{VEC} = \sum c_i \text{VEC}_i , \quad (3)$$

where VEC_i is the valence electron concentration of the ith element.

$$\Delta H_{\text{mix}} = \sum_{i<j} 4 H_{ij} c_i c_j , \quad (4)$$

where H_{ij} is the enthalpy of mixing of elements *i* and *j* at the equimolar concentration in regular binary solutions; c_i and c_j are the atom fractions of elements *i* and *j*;

$$\Delta S_{\text{mix}} = -R \sum c_i \ln c_i , \quad (5)$$

where *R* is the universal gas constant.

The design of high-entropy alloys on the basis of empirical parameters has been the subject of extensive research [63–67]. For instance, it was suggested [68] that multi-principal element alloys tend to form solid solution phases when $\delta \le 6.5\%$, $-15 \text{ kJ/mol} < \Delta H_{mix} < 5 \text{ kJ/mol}$, and $12 \text{ J/(K·mol)} < \Delta S_{mix} < 17.5 \text{ J/(K·mol)}$. The VEC parameter has been proposed to explain the formation of certain crystal packing arrangements in the resultant alloy [69]. FCC solid solution phase is more stable when VEC is greater than 8.6, while a BCC solid solution phase is more stable when VEC is less than 6.87. Within the range of 6.87–8.00, both BCC and FCC structures are observed [60].

Yang and Zhang [70] also proposed another parameter, Ω, for estimating the solid-solution formation ability in a multi-component alloy system. The parameter Ω is defined as

$$\Omega = \frac{T_m \Delta S_{\text{mix}}}{|\Delta H_{\text{mix}}|} , \quad (6)$$

where T_m is the melting temperature.

The criteria for the formation of stable solid-solution phases are $\Omega \ge 1.1$ and $\delta \le 6.6\%$. These empirical parameters represent the balance between mixing entropy and mixing enthalpy and are effective in predicting the formation of solid solutions in alloys.

Empirical parameters are recognized to help design HEA compositions for hydrogen storage. Among these parameters, atomic size mismatch δ, VEC, and electronegativity $\delta\chi$ have the strongest impact on the storage performance of hydride-forming alloys. It has been demonstrated, particularly in [71], that doping elements with high electronegativity can reduce dehydrogenation energy by nearly 25%. For instance, the hydrogen storage capacity of V-Ti-Cr-Fe alloys can be predicted by utilizing electronegativity as one of the inputs [72].

VEC parameters can also be used to predict the hydrogen storage performance of HEAs. According to Nygård et al., a lower hydrogen desorption temperature corresponds to a higher VEC, because the thermal stability of hydride is influenced by the VEC, in addition, VEC also was suggested to be helpful for predicting the hydrogen storage capacity [73]. The authors [73] also proposed that alloys with VEC < 4.75 reached maximum capacity of 2 H/M, whereas alloys with VEC > 5 presented reduced maximum capacity (H/M < 2.0), indicating the formation of non-stoichiometric hydride for these larger VEC. Moreover, it was suggested [41] that the fast hydrogen absorption/desorption performance can be obtained at room temperature when the VEC is greater than 6.4. However, achieving reversibility of hydrogen storage can be challenging, as hydrogen desorption efficiency becomes a problem when VEC is less than 6.4 [73].

Detailed analysis of the influence of empirical parameters on HEAs hydrogen storage performance has been reported recently in [74, 75]. While empirical parameters can be helpful in designing HEA compositions for hydrogen storage, it is important to note that their applicability and predictive accuracy are limited. It is also worth noting that empirical parameters may not fully account for all influencing factors, and their impact on performance may decrease as compositions become more complex.

CALPHAD. The synthesis of HEAs involves utilizing numerous elements leading to a wide array of possible alloys and combinations, thus resulting in a diverse range of properties within these materials. One effective method for predicting the constituent phases in multi-component systems, including HEAs, is the Calculation of Phase Diagram (CALPHAD) approach. This approach has demonstrated significant capability in

predicting phase structures and is particularly relevant for applications such as hydrogen storage, where the properties are highly dependent on the alloy's phase structure [41, 49, 70, 76]. By employing the CALPHAD approach, it is possible to predict favorable phase structures conducive to storing large amounts of hydrogen. The computational phase diagram generated by the CALPHAD model assists in the design process by assessing the phase equilibrium relationships within the system based on thermodynamic parameters. To accurately predict phase equilibria in multi-component alloys and design new hydrogen storage materials, it is essential to construct a comprehensive database. Currently, the prediction of phase structures in HEAs is primarily based on extrapolation from thermodynamic evaluations of simpler metal-hydrogen systems, including binary and ternary systems. Nevertheless, studies have shown a strong correlation between predicted phase structures and experimental results. For instance, the CALPHAD method was successfully used [77] to design compositions with different phase structures (BCC and Laves phases) in the TiVNbCr system. The accuracy of these predictions was confirmed by X-ray diffraction (XRD) analysis of the different phase structures. Similarly, in another study [78] three compositions of the TiVNbCr system with a BCC single phase were designed using the CALPHAD approach, and the phase diagram predictions were verified by XRD experiments with high precision. As the demand for applications utilizing HEAs continues to grow, there is a corresponding expansion in the utilization of theoretical calculations as a design approach, further emphasizing the importance and applicability of the CALPHAD method in materials science research and development.

First-principles calculations. Density functional theory (DFT) is a computational method widely employed in the design of high-entropy alloys with favorable hydrogen storage properties. For instance, DFT has been used to determine the enthalpy of formation of single and multi-principal element hydrides through total energy calculations [79–82]. In addition, DFT was utilized to design a BCC single-phase TiZrHfScMo alloy, which was predicted to accommodate 2.14 wt.% H_2 and subsequently TiZrVMoNb alloy with a maximum hydrogen storage capacity of 2.65 wt.% [83, 84]. These researches contributed significantly to the development of alloys with high reversible hydrogen storage capacities. According to [32, 33], a key challenge in designing room-temperature hydrogen storage materials is adjusting the hydrogen binding energy to a negative value close to zero. Previous studies on first-principles calculations of Mg-based alloys suggested that binding energies of approximately -0.1 eV per hydrogen atom could be an appropriate target for achieving room temperature hydrogen storage. In a recent study [33], high-entropy alloys capable of storing hydrogen at room temperature and under pressures close to atmospheric were successfully designed and synthesized. Specifically, $Ti_xZr_{2-x}CrMnFeNi$ (x = 0.4–1.6) alloys were theoretically designed using first-principles calculations. These alloys, with low hydrogen binding energies (negative values close to -0.1 eV), were then fabricated experimentally. They exhibited the ability to reversibly absorb and desorb up to 1.7 wt.% of hydrogen at room temperature (298 K) with fast kinetics, representing remarkable progress in the development of efficient room-temperature hydrogen storage materials.

Machine learning. Although empirical methods for estimating the enthalpy of hydride formation and other thermodynamic parameters have been used successfully for several decades, today the most effective approach to studying the thermodynamic properties of many alloys is a combination of computational thermodynamics and machine learning (ML). The growing amount of scientific research data has led to the use of ML as an efficient method for discovering complex relationships in material databases. Recent advances in ML have demonstrated its potential for screening the new hydrogen storage materials, predicting hydrogenation enthalpy, evaluating storage capacity, and optimizing process parameters. Regression algorithms are often utilized in solid-state hydrogen storage due to their ability to precisely determine values for unknown samples. For example, Witman et al. trained gradient boosting regression (GBR) to predict equilibrium plateau pressure, enthalpy, and entropy of hydride formation using features generated by the Magpie code [85]. Their results suggest that metal hydride equilibrium plateau pressure depends significantly on a volume-based descriptor. The model was later updated with more data and relevant features for screening of HEAs, successfully predicting properties for 674 equimolar HEAs of refractory elements. Suwarno et al. trained models to investigate the effect of alloying elements on the properties of AB_2 alloys, showing that Ni controls the enthalpy of hydride formation, Cr determines the phase fraction of the Laves phase C14, and Mn influences the hydrogen weight percentage (wt.% H_2) [86]. Additionally, a composition-specific ensemble learning method was developed to predict the wt.% H_2 of V–Ti–Cr–Fe alloys with high accuracy [87]. The model, trained on 19 features, was able to predict wt% H_2 with a mean absolute error of 0.187 wt.%. Recently, an ML framework HEART was presented for identifying metal alloy families suitable for hydrogen storage at ambient conditions [88]. HEART includes models that predict hydrogen storage capacity (HYST) and enthalpy of hydride formation (THOR) for multi-component metal alloys. These models were used to predict wt.% H_2 and ΔH for 6.4 million multi-component metal alloys. The authors have identified 6480 compositions with superior storage properties (wt.% $H_2 > 2.5$ and $\Delta H < 60$ kJ/molH_2) having potential for hydrogen storage at room temperature.

While there are currently limited works employing computational methods, such as DFT and ML, the future of HEAs design for hydrogen storage depends on evaluating the thermodynamic properties of various systems using computational techniques. This approach is expected to significantly minimize the need for extensive experimental trials.

4. HYDROGEN STORAGE PERFORMANCE OF SELECTED HEAS

Among reported hydrogen storage compositions for HEAs, BCC, and Laves phase alloys are generally recognized to be more favorable for hydride formation. These phases exhibit improved hydrogen absorption and desorption kinetics, making them attractive for efficient hydrogen storage systems.

4.1. BCC HEAs

BCC HEAs have been extensively investigated in the field of solid-state hydrogen storage, with several alloy compositions demonstrating promising performance. The development of compositional design methods has the potential to greatly advance the synthesis of BCC HEAs with reversible hydrogen storage capabilities. The majority of BCC HEAs explored for hydrogen storage have been synthesized using the arc melting method, which aids in achieving alloy homogeneity and retaining solid solution structures.

Hydrogen Capacity. Upon hydrogenation BCC HEAs often exhibit hydrogen-to-metal ratios as high as 2, while some studies have shown that certain BCC HEA compositions can achieve H/M ratios exceeding 2. Sahlberg et al. [89] succeeded in attaining a high hydrogen-to-metal ratio of 2.5 (equivalent to only 2.7 wt.% due to the high molecular weight of the alloying elements) through the hydrogenation of a TiVZrNbHf-based HEA. This exceptional capacity was attributed to the occupation of both tetrahedral and octahedral sites in the hydride body-centered tetragonal (BCT) structure, enabled by significant lattice distortions. However, subsequent efforts with a series of HEAs in the same TiVZrNbHf system [46] as well as the similar TiZrNbHfTa system [90] did not reproduce this high ratio. All these alloys form hydrides when exposed to gaseous hydrogen with hydrogen-to-metal ratios of up to 2.0. Moreover, no correlation was found between the atomic size mismatch and hydrogen storage capacity [46]. Meanwhile, recent studies [21, 22] have reported a hydrogen capacity of 3.7 wt.% in the $Ti_{35}V_{30}Nb_{10}Cr_{25}$ and $Ti_4V_3NbCr_2$ alloys, which appear to be the highest hydrogen capacity reported for BCC-structured HEAs to date. This demonstrates the potential for high hydrogen storage performance in BCC alloys. Other investigations, such as the development of $MgZrTiFe_{0.5}Co_{0.5}Ni_{0.5}$ [65] and $Mg_{12}Al_{11}Ti_{33}Mn_{11}Nb_{33}$ [91] alloys, have yielded hydrogen capacities ranging from 1.2 to 1.75 wt.%, demonstrating the diverse hydrogen storage properties observed in different alloy compositions.

Neutron diffraction studies on deuterated TiVZrNbHf HEAs have confirmed the occupancy of both tetrahedral and octahedral sites by deuterium. According to [46, 92], deuterium occupancy in tetrahedral and octahedral sites varies in different HEAs, including TiVZrNbHf, depending on temperature and pressure conditions.

Theoretical approach using density functional theory calculations on TiZrHfMoNb alloy [93] showed that at low hydrogen concentrations, octahedral sites in the BCC phase are primarily occupied, while above 1.08 wt.% H_2, there is a preference for tetrahedral sites in the FCC phase. Experimental findings support these results, indicating initial occupancy of both interstitial sites in the BCC phase and predominant occupation of tetrahedral interstices in the FCC phase at high deuterium content for TiVZrNbHf, $TiV_{0.5}ZrNbHf$, and TiVZrNb alloys [46]. Furthermore, studies [46, 73] have suggested that the formation of BCT or FCC hydrides in HEAs may be influenced by the amount of Zr and Hf, as well as the valence electron concentration. Lower VEC (< 4.4) HEAs exhibit a one-step hydrogen absorption mechanism with a BCC to BCT phase transition, while those with higher VEC (≥ 4.4) form hydrides in an FCC phase [73]. In subsequent work [94], HEAs with different alloying elements, but the same VEC of 4.87 were designed and carefully analyzed. It was observed that despite varying chemical compositions, these alloys exhibited similar hydrogenation properties. This observation suggests that VEC may influence hydride structure, emphasizing its importance in determining the properties of solid-state hydrogen storage materials.

Activation. Typically, BCC structured HEAs require activation through hydrogen absorption/desorption cycles conducted at elevated temperature and pressure to enable hydrogen absorption at ambient conditions [18, 46, 66, 73]. A study [46] investigated a number of TiVZrNbHf-based HEAs. The results indicate that most of the samples were activated at 613 K for 2 h in dynamic vacuum, while some of these alloys required activation at 773 K due to very slow hydrogen absorption kinetics. Another detailed study [24] on the activation of the TiZrNbTa alloy for hydrogen absorption showed a notable decrease in hydrogen absorption temperature (from 715 to 300 K) following three hydrogen absorption/desorption cycles at high temperatures. To explain this process, a two-stage activation mechanism has been proposed: the first stage involves the reduction of surface oxides to sub-oxides, followed by the conversion of the sub-oxides to sub-hydroxides. The authors emphasized the greater importance of sub-hydroxide formation over sub-oxide effects on the activation and hydrogen absorption temperature of HEAs, attributing this to the easy diffusion of hydrogen atoms within sub-hydroxides. The investigation of TiVZrHfNb HEA [95] showed that the first hydrogenation is significantly affected by particle size, pressure and temperature. Smaller particle sizes resulted in faster kinetics, while higher temperatures reduced the incubation time, indicating the importance of temperature in activation process.

Hydrogenation/dehydrogenation behavior. The hydrogenation kinetics of HEAs is often characterized by the time required for the alloy to reach 90% of its maximum hydrogen storage capacity. Recent studies have demonstrated that HEAs can achieve nearly full hydrogen storage capacity within remarkably short time frames, ranging from seconds to minutes. For instance, Ti-V-Nb-based alloys [94] can achieve a 2 H/M ratio in less than a minute at room temperature, while TiVCrFe alloys [96] reach hydrogen saturation in approximately 125 seconds. In addition, the $Ti_{0.30}V_{0.25}Zr_{0.10}Nb_{0.25}Ta_{0.10}$ alloy [18] was found to absorb 2 H/M within two minutes at 373 K under 3.3 MPa of H_2. Furthermore, the

kinetic data of TiZrNbTa alloys [97] have been shown to be consistent with the Johnson-Mehl-Avrami equation, indicating that the hydrogenation kinetics can be interpreted in terms of nucleation and growth mechanisms. Among the factors influencing hydrogenation kinetics, the effect of particle size has been noted [95], showing that alloys with smaller particle sizes (< 0.5 mm) exhibit faster kinetics, although a definitive correlation between particle size and kinetics remains unclear and requires further research.

The dehydrogenation behavior of hydrogenated BCC alloys has been extensively studied, revealing a complex interplay between alloy composition and hydrogen desorption properties. Most BCC HEAs exhibit high desorption temperatures, usually around 500 K or higher, indicating the formation of stable hydride phases [12]. In addition, the multistage desorption has been observed in various alloys with different chemical compositions [18, 46, 66]. For instance, Ti–V–Zr–Nb–Hf-based alloys exhibit a two-stage hydrogen absorption/desorption reaction. It was found that the onset temperature of the first stage remains relatively stable, while the second stage temperature decreases linearly with increasing VEC. Although phenomenon of multistage desorption in BCC HEAs remains unclear, potential explanations, such as hydrogen jump between tetrahedral and octahedral sites have been proposed [46]. Changes in composition or the addition of alloying elements can significantly alter hydrogen desorption properties. Dehydrogenation of TiZrHfMoNb system alloys with varying Mo contents revealed a decrease in hydride desorption temperature from 656 to 437 K with increasing Mo content [44]. The decrease in hydride thermal stability was attributed to a decrease in the radius of the interstitial site housing the hydrogen atom, and DFT calculations [84] confirmed that altering Mo content weakens the alloy-H bonding, thereby reducing the thermal stability of the hydride. In another study [94], the addition of Cr, Co, or Ni to Ti-V-Nb-based alloys improves significantly hydrogen desorption behavior with reduced onset temperatures in the range of 324…409 K, potentially due to the limited hydride formation capability of these elements.

Cycling. For most applications, compositions with better reversible hydrogen storage capacity are more valuable than high hydrogen capacity alone, which may introduce a broader approach to performance tuning. The critical aspect of investigating of BCC HEAs cyclic performance is to mitigate the cyclic decay of the effective hydrogen storage capacity. These alloys show differing behaviors in their cyclic performance, as demonstrated by their capacity decay rates over multiple cycles. Ti-V-Nb-based alloys [94] show a slight decrease in hydrogen storage capacity during cycling due to increased defects and loss of crystallinity, but the capacity stabilizes after a few cycles. TiZrNbTa alloy's capacity decreased from 1.6 to 1.38 wt.% after ten cycles, attributed to particle pulverization and increased defect density [97]. The $V_{0.3}Ti_{0.3}Cr_{0.25}Mn_{0.1}Nb_{0.05}$ high-entropy alloy [45] can absorb hydrogen at room temperature without incubation time and reaches a maximum hydrogen storage capacity of 3.45 wt.%. But after five cycles, the capacity retention of alloy was less than half of the initial capacity. The hydrogen absorption capacity decreases with cycling due to high hydride stability and incomplete desorption at room temperature. The studies [98] of the $(VFe)_{60}(TiCrCo)_{40-x}Zr_x$ alloys have also demonstrated that the alloys absorb around 3.5 wt.% H_2 at room temperature while only 1.88…2.1 wt.% H_2 is reversible. Moreover, the reversible capacity of alloy was reduced by 4.5…10.9% upon cycling. The authors proposed the accumulation of micro-strains as a reason for the deterioration of reversible hydrogen storage capacity. In order to improve the hydrogen storage efficiency of BCC-structured HEAs, attention should be focused on improving the cycling properties of the material. This goal can be achieved by careful selection of alloying elements. Specifically, the addition of Mg into Ti-V-Zr-Nb-based HEAs was shown [58] to improve the hydrogen cycling properties, stabilizing the reversible hydrogen storage from the second cycle with a slight decay from 2.7 to 2.4 wt.%. The authors concluded that good compositional homogeneity is a key factor in the enhanced cycling performance of the alloy.

Table 1 summarizes the hydrogen storage properties of several BCC HEAs with a maximum storage capacity exceeding 2.5 wt.%.

Table 1

Hydrogen storage properties of selected BCC HEAs

HEA composition	Synthesis method	Alloy phase\ Hydride phase	H_2 storage capacity, max/revers., wt.%	H/M	T_{absorp}/ $T_{onset\ desorp.}$, K	VEC	Refs.
TiVZrNbHf	AM	BCC→ BCT	2.7/-	2.5	298/473	4.40	[89]
$Mg_{0.10}Ti_{0.30}V_{0.25}Zr_{0.10}Nb_{0.25}$	BM	BCC→ FCC	2.7/2.4	1.7	298/523	4.30	[58]
$Al_{0.10}Ti_{0.30}V_{0.25}Zr_{0.10}Nb_{0.25}$	AM	BCC→ BCT	2.6/2.45	1.6	298/323	4.40	[99]
$Ti_{0.30}V_{0.25}Cr_{0.10}Zr_{0.10}Nb_{0.25}$	AM	BCC →FCC	3.0/2.44	2.0	298/458	4.7	[49]
TiZrVMoNb	–	BCC→ FCC	2.65/-	2.05	–	4.8	[84]
$(TiVNb)_{85}Cr_{15}$	AM	BCC →FCC	3.18/2.88	2.0	298/436	4.87	[94]
$(TiVNb)_{95.3}Co_{4.7}$	AM	BCC →FCC	3.11/2.77	2.0	298/483	4.87	[94]
$(TiVNb)_{96.2}Ni_{3.8}$	AM	BCC→ FCC	3.17/2.77	1.9	298/483	4.87	[94]
$V_{0.3}Ti_{0.3}Cr_{0.25}Mn_{0.1}Nb_{0.05}$	AM	BCC→ FCC	3.45/1.78	–	298/-	–	[45]
$Ti_4V_3NbCr_2$	AM	BCC→ FCC	3.7/-	2.01	300/600	5,0	[22]
$Ti_{27.5}V_{27.5}Nb_{20}Cr_{12.5}Mn_{12.5}$	AM	BCC→ FCC	3.38/2.2	2.1	298/-	5.1	[100]
$Ti_{35}V_{30}Nb_{10}Cr_{25}$	AM	BCC →FCC	3.72/-	2.0	300/-	–	[21]

The majority of hydrogen storage alloys with high hydrogen capacity face the issue of hydrogen desorption. Thus, future efforts to enhance the hydrogen storage performance of BCC-structured HEAs should focus on reducing the desorption temperature and enhancing the cyclic performance.

4.2. LAVES PHASE HEAs

High-entropy alloys with a C14 Laves phase structure have gained significant interest as potential hydrides for solid-state storage due to their impressive hydrogen storage capacity at room temperature, fast kinetics, and excellent reversibility, all without the need for a complicated activation procedure [33, 41, 101–105]. The most commonly used elements for the formation Laves phase alloys are Ti and Zr, thus, they have been widely used in the study of HEAs for hydrogen storage, while other transition metals, including V, Cr, Fe, and Mn, have also been used to create multi-principal element systems. The majority of Laves phase HEAs studied for hydrogen storage have been synthesized using the arc melting method, which was found to be effective in achieving alloy homogeneity. Recently, certain selection criteria have been proposed to develop prospective multicomponent alloys with a C14 Laves phase structure for room temperature hydrogen storage. These include a valence electron concentration of 6.4, single-phase thermodynamic stability, and low hydrogen binding energy (slightly more negative than -0.1 eV) [33, 106].

Hydrogen Capacity. The first approach related to hydrogen storage in Laves phase HEAs was made by Kao et al. [20]. The authors systematically investigated the influence of Ti, V, and Zr contents in the $CoFeMnTi_xV_yZr_z$ alloy system ($0.5 \le x \le 2.5$, $0.4 \le y \le 3.0$, and $0.4 \le z \le 3.0$) on the hydrogen absorption – desorption performance. After synthesis via vacuum arc melting, all the alloys showed a C14 Laves structure. Upon hydrogenation, the alloys have remained C14 Laves structure and the H_2 uptake leads to expansion of the structure. The highest hydrogen absorption was observed in the $CoFeMnTi_2VZr$ and $CoFeMnTiVZr_{2.3}$ alloys, with a hydrogen adsorption capacity of 1.80 and 1.79 wt.%, respectively.

The AB_2-type hydrides typically have a hydrogen storage capacity of $AB_2H_{3–4}$ and are characterized by a relatively high gravimetric storage capacity (up to 2…2.5 wt.% H_2) [107]. The hydrogen storage performance results reported for the investigated intermetallic HEAs are generally similar to those of traditional intermetallic compounds. The maximum hydrogen storage capacity of the alloys investigated so far ranges from 0.03 to 2.23 wt.% H_2. The reported values for H/M are between 0.02 and 1.17 [12].

Activation. HEAs with the C14 Laves phase have shown a high potential for reversible hydrogen storage, even at room temperature. However, some of these alloys require a high-temperature activation [18, 41, 44, 46, 58, 95, 90]. Recent research has focused on addressing this issue, with some studies [108, 109] in particular offering promising solutions. For instance, the study [108] examined the role of interphase boundaries in facilitating the easy activation of HEAs at room temperature. For this purpose, two chemically similar HEAs were synthesized: $TiV_{1.5}Zr_{1.5}CrMnFeNi$, a single-phase alloy with only the C14 phase, and $TiV_{1.5}ZrCr_{0.5}MnFeNi$, a dual-phase alloy with C14 and 4 vol.% BCC phases. The dual-phase alloy demonstrated the ability to readily absorb hydrogen at room temperature without any activation treatment, while the single-phase alloy required high-temperature activation. This suggests that interphase boundaries provide pathways for easy hydrogen transport and activation at room temperature. Studies [108, 109] highlight the generation of interphase boundaries as an effective strategy to overcome the activation drawback of Laves phase HEAs.

Hydrogenation/dehydrogenation behavior. The majority of the Laves phase alloys examined exhibit fast hydrogen absorption/desorption kinetics [12]. The kinetic increases with increasing concentrations of Cr, Fe, and Mn, but it decreases with higher Zr content. The decrease in kinetics observed with Zr is attributed to its larger atomic size compared to other atoms, which facilitates hydrogen diffusion [110]. Meanwhile, research papers often highlight the issue of segregation of certain elements, such as Ti and Zr, which can negatively impact the absorption capacity of alloys by reducing regions susceptible to hydrogen absorption due to the formation of oxides by the segregated elements [12].

Cycling. The absorption/desorption cycling properties of hydrogen storage materials are crucial for their practical applications. Some elements in HEA compositions have a strong affinity for hydrogen, leading to high enthalpies of hydride formation. As a result, hydrogen can retain within the structure of HEAs even after absorption/desorption cycles, significantly limiting these alloys' reversible capacity. Meanwhile, the hydrogen storage behavior and properties of these alloys can be significantly adjusted by modifying their chemical composition, thereby enhancing the reversible storage capacity [20, 40]. Recent advancements have been made in this area, particularly in the development of HEAs with a single C14 Laves phase [33, 41, 49, 102]. Chen et al. [102] prepared a six-element HEA, TiZrFeMnCrV, using arc melting and mechanical milling. This alloy demonstrated ultra-fast hydrogen-absorption kinetics, absorbing 1.80 wt.% of hydrogen at 303 K. Notably, the hydrogen-storage capacity remained stable at 1.76 wt.% over 50 cycles, with 90% of hydrogen absorbed in 60 s, indicating excellent reversible hydrogen storage performance. Additionally, Mohammadi et al. [33] synthesized a series of $Ti_xZr_{2-x}CrMnFeNi$ (x = 0.4–1.6) alloys with a C14 Laves phase. The $Ti_{0.4}Zr_{1.6}CrMnFeNi$ alloy exhibited outstanding performance, with its hydrogen-storage capacity remaining virtually unchanged throughout the cycling process. The pressure-composition isotherms of this alloy remained consistent even after the 1000th cycle. These studies illustrate promising advancements in the cycling performance of C14 Laves phase HEAs in the field of hydrogen storage.

Hydrogen storage properties of several Laves phase HEAs are shown in Table 2.

Table 2

Hydrogen storage properties of selected Laves phase HEAs

HEA composition	Synthesis method	Alloy phase\ Hydride phase	H_2 max. storage Capacity, wt.%	H/M	T_{absorp}, K	VEC	Refs.
$CoFeMnTiVZr_{2.3}$	AM	C14→C14	1.79	1.21	298	5.78	[20]
CrMnTiVZr	AM	C14→C14	2.23	1.34	278	7.49	[40]
TiZrCrMnFeNi	AM	C14→C14	1.7	1.03	303	6.50	[41]
TiZrFeMnCrV	AM	C14→C14	1.80	1.1	303	5.8	[102]
TiZrVCrNi	AM	C14→C14	1.52	0.92	305	5.80	[111]
TiZrNbFeNi	AM	C14→C14	1.64	1.17	305	6.20	[49]
$Zr_{22.5}Ti_{22.5}V_{22.5}Fe_{22.5}Al_{10}$	AM	C14→C14	1.4	0.76	423	5.03	[47]
$Zr_{0.2}Ti_{0.2}Ni_{0.2}Cr_{0.2}Mn_{0.2}$	AM	C14→C14	1.66	0.92	323	6.00	[112]
$Ti_{0.4}Zr_{1.6}CrMnFeNi$	AM	C14→C14	1. 7	1.06	298	6.40	[33]
$Ti_{0.8}Zr_{1.2}CrMnFeNi$	AM	C14→C14	1.6	1.0	298	6.40	[33]

In conclusion, although Laves phase HEAs do not appear to exhibit notably superior hydrogen storage behavior compared to other Zr/Ti-based Laves phase alloys, they could serve as promising candidates for hydrogen absorption and desorption at room temperature, demonstrating fast kinetics without requiring activation treatment.

SUMMARY

High-entropy alloys have shown promising hydrogen storage properties, including storage capacity, reversibility, kinetics, and cyclability. These properties can be further enhanced by compositional modification and improvements in preparation or activation methods. However, additional investigations are needed to better understand the kinetics of hydrogen-surface/matrix interactions in these alloys, as research in this area is currently limited. Modern theoretical methods, such as CALPHAD and DFT computations, are increasingly guiding the development of HEAs for hydrogen storage. These predictive methods are crucial for correlating alloy composition with hydrogen storage properties. The implementation of machine learning techniques could further advance this field of materials science.

The BCC HEAs have been found to have the greatest potential for hydrogen storage, with further research needed to reduce their desorption temperature and improve the cyclic performance. Laves phase HEAs have also demonstrated the ability to reversibly absorb large amounts of hydrogen at room temperature without requiring an activation process, suggesting potential for further investigation, particularly of HEAs with C14 Laves structure.

Despite these advancements, research on hydrogen storage in HEAs is still in its early stages, and many issues related to the hydrogen storage properties of these alloys remain to be addressed. Further improvements in alloy composition, preparation process, and hydrogen storage performance are required to achieve commercial viability.

ACKNOWLEDGEMENTS

The author would like to acknowledge funding for this research from the Petersen Institute of NanoScience and Engineering at the University of Pittsburgh.

REFERENCES

1. J.B. von Colbe, J.R. Ares, J. Barale, M. Baricco, C. Buckley, G. Capurso, N. Gallandat, D.M. Grant, M.N. Guzik, I. Jacob, E.H. Jensen, T. Jensen, J. Jepsen, T. Klassen, M.V. Lototskyy, K. Manickam, A. Montone, J. Puszkiel, S. Sartori, D.A. Sheppard, A. Stuart, G. Walker, C.J. Webb, H. Yang, V. Yartys, A. Zuttel, M. Dornheim. Application of hydrides in hydrogen storage and compression: Achievements, outlook and perspectives // *Int. J. Hydrogen Energy*. 2019, v. 44, p. 7780-7808.
2. Udo Energy. DOE technical targets for Onboard hydrogen storage for light-duty vehicles: DOE U; 2021.
3. M.M. Nygård, Ø.S. Fjellvåg, M.H. Sørby, K. Sakaki, K. Ikeda, J. Armstrong, P. Vajeeston, W.A. Sławiński, H. Kim, A. Machida, Y. Nakamura, B.C. Hauback. The average and local structure of $TiVCrNbD_x$ (x=0, 2. 2, 8) from total scattering and neutron spectroscopy // *Acta Mater*. 2021, v. 205, p. 116496.
4. C. Frommen, M.H. Sørby, M. Heere, T.D. Humphries, J.E. Olsen, B.C. Hauback. Rare earth borohydrides – Crystal structures and thermal properties // *Energies*. 2017, v. 10(12), p. 2115.
5. J.G. Yuan, J.T. Chen, H.X. Huang, Y.J. Lv, B. Liu, Z. Li, B. Zhang, W. Lv, Y. Wu. Enhanced hydrogen storage properties of $NaBH_4$–$Mg(BH_4)_2$ composites by NdF_3 addition // *Prog. Nat. Sci*. 2021, v. 31, p. 521-526.
6. G.I. Duarte, L.A.C. Bustamante, P.E.V. de Miranda. Hydriding properties of an Mg-Al-Ni-Nd hydrogen storage alloy // *Scr. Mater*. 2007, v. 56, p. 789-792.
7. J.A. Puszkiel, F.C. Gennari. Reversible hydrogen storage in metal-doped Mg–$LiBH_4$ composites // *Scr. Mater*. 2009, v. 60, p. 667-670.
8. J.M. Joubert, M. Latroche, A. Percheron-Guégan. Hydrogen absorption properties of several intermetallic compounds of the ZrNi system // *J. Alloy. Compd*. 1995, v. 231, p. 494-497.
9. L. Schlapbach, T. Riesterer. The activation of FeTi for hydrogen absorption // *Appl. Phys. A.* 1983, v. 32, p. 169-182.
10. E.M. Dematteis, N. Berti, F. Cuevas, M. Latroche, M. Baricco. Substitutional effects in TiFe for hydrogen storage: a comprehensive review // *Mater. Adv*. 2021, v. 2, p. 2524-2560.

11. R. Cohen, K. West, J. Wernick. Degradation of LaNi5 by temperature-induced cycling // *J. Less-Common Met*. 1980, v. 73, p. 273-279.

12. F. Marques, M. Balcerzak, F. Winkelmann, G. Zepon, M. Felderhoff. Review and outlook on high-entropy alloys for hydrogen storage // *Energy Environ Sci*. 2021, v. 14, p. 5191-5227.

13. B. Cantor, I.T.H. Chang, P. Knight, A.J.B. Vincent. Microstructural development in equi-atomic multicomponent alloys // *Mater. Sci. Eng. A* 2004, v. 375-377, p. 213-218.

14. J.-W. Yeh, S.-K. Chen, S.-J. Lin, J.-Y. Gan, T.-S. Chin, T.-T. Shun, C.-H. Tsau, S.-Y. Chang. Nanostructured high-entropy alloys with multiple principal elements: novel alloy design concepts and outcomes // *Adv. Eng. Mater*. 2004, v. 6, p. 299-303.

15. E.J. Pickering, N.G. Jones. High-entropy alloys: a critical assessment of their founding principles and future prospects // *Int. Mater. Rev*. 2016, v. 61(3), p. 183-202.

16. R.R. Shahi, R.K. Mishra. High entropy alloys; A potential Magnetic materials. In: Srivatsan TS, Gupta M, editors. High entropy alloys innovation, advance and applications. CRC Press; July 2020, p. 655-688.

17. M.H. Tsai, J.W. Yeh. High-entropy alloys: a critical review // *Mater. Res. Lett*. 2014, v. 2(3), p. 107-123.

18. J. Montero, G. Ek, L. Laversenne, V. Nassif, G. Zepon, M. Sahlberg, C. Zlotea. Hydrogen storage properties of the refractory Ti-V-Zr-Nb-Ta multi-principal element alloy // *J. Alloys Compd*. 2020, v. 835, p. 155376.

19. J. Montero, C. Zlotea, G. Ek, J.C. Crivello, L Laversenne, M. Sahlberg. TiVZrNb multi-principal-element alloy: synthesis optimization, structural, and hydrogen sorption properties // *Molecules*. 2019, v. 24, p. 2799.

20. Y.F. Kao, S.K. Chen, J.H. Sheu, J.T. Lin, W.E. Lin, J.W. Yeh, S.J. Lin, T.H. Liou, and C.W. Wang. Hydrogen storage properties of multi-principal-component $CoFeMnTi_xV_yZr_z$ alloys // *Int. J. Hydrogen Energy*. 2010, v. 35, p. 9046-9059.

21. B. Cheng, L. Kong, Y. Li, D. Wan, Y. Xue. Hydrogen desorption kinetics of $V_{30}Nb_{10}(Ti_xCr_{1-x})_{60}$ high-entropy alloys // *Metals*. 2023, v. 13, p. 230.

22. B. Cheng, Y. Li, X. Li, H. Ke, L. Wang, T. Cao, D. Wan, B. Wang, Y. Xue. Solid-state hydrogen storage properties of Ti-V-Nb-Cr high-entropy alloys and the associated effects of transitional metals (M = Mn, Fe, Ni) // *Acta Metall. Sin*. 2023, v. 36, p. 1113-1122.

23. A. Züttel. Materials for Hydrogen Storage // *Mater. Today*. 2003, v. 6, p. 24-33.

24. C. Zhang, Y. Wu, L. You, X. Cao, Z. Lu, X. Song. Investigation on the activation mechanism of hydrogen absorption in TiZrNbTa high entropy alloy // *J. Alloys Compd*. 2019, v. 781, p. 613-620.

25. P.E. de Jongh. Hydrogen storage: keeping out the oxygen // *Nat. Mater*. 2011, v. 10, p. 265-266.

26. C. Yin, W. Li, X. Qiu, B. Luo, H. Huang. Characterization of the oxide film and deuterium permeation behavior of CoCrMnFeNi high entropy alloy oxidized at 550 °C for 24 h // *Mater. Lett*. 2023, v. 347, p. 134632.

27. M. Williams, M.V. Lototsky, M.W. Davids, V. Linkov, V.A. Yartys, J.K. Solberg. Chemical surface modification for the improvement of the hydrogenation kinetics and poisoning resistance of TiFe // *J. Alloys Compd*. 2011, v. 509, p. S770-S774.

28. T. Akiyama, K. Saito, I. Saita. Kinetic improvement of hydrogen storage alloy by generating nanofissures // *J. Electrochem. Soc*. 2003, v. 150, p. E450-E454.

29. D. Pukazhselvan, I. Bdikin, J. Perez, E. Carbo-Argibay, I. Antunes, D.G. Stroppa, D.P. Fagg. Formation of Mg-Nb-O rock salt structures in a series of mechanochemically activated $MgH_2 + nNb_2O_5$ (n = 0.083–1.50) mixtures // *Int. J. Hydrogen Energy*. 2016, v. 41, p. 2677-2688.

30. O. Friedrichs, D. Martínez-Martínez, G. Guilera, J.C.S. Lopez, A. Fernandez. In situ energy-dispersive XAS and XRD study of the superior hydrogen storage system MgH_2/Nb_2O_5 // *J. Phys. Chem. C*. 2007, v. 111, p. 10700-10706.

31. W. Li, B. Luo, H. Huang, Y. Liu, W. Wang, J. Luo, B. Fu. A comparative study of deuterium permeation behaviors of CoCrMnFeNi and AlCoCrFeNi high entropy alloys // *Int. J. Hydrogen Energy*. 2023, v. 48, p. 19657-19665.

32. K. Edalati, R. Uehiro, Y. Ikeda, H.W. Li, H. Emami, Y. Filinchuk, M. Arita, X. Sauvage, I. Tanaka, E. Akiba, Z. Horita. Design and synthesis of a magnesium alloy for room temperature hydrogen storage // *Acta Mater*. 2018, v. 149, p. 88-96.

33. A. Mohammadi, Y. Ikeda, P. Edalati, M. Mito, B. Grabowski, H.W. Li, K. Edalati. High-entropy hydrides for fast and reversible hydrogen storage at room temperature: Binding-energy engineering via first-principles calculations and experiments // *Acta Mater*. 2022, v. 236, p. 118117.

34. M. Dornheim. Tailoring reaction enthalpies of hydrides. In: Hirscher M, editor. Handbook of hydrogen storage. Weinheim: WILEY-VCH Verlag GmbH &Co. KGaA; 2010, p. 187-214.

35. Y. Zhang, T.T. Zuo, Z. Tang, M.C. Gao, K.A. Dahmen, P.K. Liaw, Z.P. Lu. Microstructures and properties of high-entropy alloys // *Prog. Mater. Sci*. 2014, v. 61, p. 1-93.

36. W. Zhang, P.K. Liaw, Y. Zhang. Science and technology in high-entropy alloys // *Sci. China Mater*. 2018, v. 61, p. 2-22.

37. H. Prasad, S. Singh, B.B. Panigrahi. Mechanical activated synthesis of alumina dispersed FeNiCoCrAlMn high entropy alloy // *J. Alloy Compd*. 2017, v. 692, p. 720-726.

38. W. Ji, Z. Fu, W. Wang, H. Wang, J. Zhang, Y. Wang, F. Zhang. Mechanical alloying synthesis and spark plasma sintering consolidation of CoCrFeNiAl high-entropy alloy // *J. Alloy Compd*. 2014, v. 589, p. 61-66.

39. X. Wang, W. Guo, Y. Fu. High-entropy alloys: emerging materials for advanced functional applications // *J. Mater. Chem*. 2021, v. 9, p. 663-701.

40. S.K. Chen, P.H. Lee, H. Lee, and H.T. Su. Hydrogen storage of C14-$Cr_uFe_vMn_wTi_xV_yZr_z$ alloys // *Mater. Chem. Phys*. 2018, v. 210, p. 336-347.

41. P. Edalati, R. Floriano, A. Mohammadi, Y. Li, G. Zepon, H.W. Li, K. Edalati. Reversible room temperature hydrogen storage in high-entropy alloy TiZrCrMnFeNi // *Scripta Mater*. 2020, v. 178, p. 387-390.

42. R.B. Strozi, D.R. Leiva, G. Zepon, W.J. Botta, J. Huot. Effects of the chromium content in $(TiVNb)100_xCr_x$ body-centered cubic high entropy alloys designed for hydrogen storage applications // *Energies*. 2021, v. 14, p. 3068.

43. H. Shen, J. Zhang, J. Hu, J. Zhang, Y. Mao, H. Xiao, X. Zhou, X. Zu. A novel TiZrHfMoNb high-entropy alloy for solar thermal energy storage // *Nanomaterials*. 2019, v. 9, p. 248.

44. H. Shen, J. Hu, P. Li, G. Huang, J. Zhang, J. Zhang, Y. Mao, H. Xiao, X. Zhou, X. Zu, X. Long, S. Peng. Compositional dependence of hydrogenation performance of Ti-Zr-Hf-Mo-Nb high-entropy alloys for hydrogen/tritium storage // *J. Mater. Sci. Technol*. 2020, v. 55, p. 116-125.

45. J. Liu, J. Xu, S. Sleiman, F. Ravalison, W. Zhu, H. Liu, H. Cheng, J. Huot. Hydrogen storage properties of $V_{0.3}Ti_{0.3}Cr_{0.25}Mn_{0.1}Nb_{0.05}$ high entropy alloy // *Int. J. Hydrogen Energy*. 2022, v. 47, p. 25724-25732.

46. G. Ek, M.M. Nygård, A.F. Pavan, J. Montero, P.F. Henry, M.H. Sørby, M. Witman, V. Stavila, C. Zlotea, B.C. Hauback, M. Sahlberg. Elucidating the effects of the composition on hydrogen sorption in TiVZrNbHf-based high-entropy alloys // *Inorg. Chem*. 2021, v. 60, p. 1124-1132.

47. X. Ma, X. Ding, R. Chen, X. Gao, Y. Su, H. Cui. Enhanced hydrogen storage properties of $ZrTiVAl_{1-x}Fe_x$ high-entropy alloys by modifying the Fe content // *RSC Adv*. 2022, v. 12, p. 11272-11281.

48. A. Bouzidi, L. Laversenne, V. Nassif, E. El-kaim, C. Zlotea. Hydrogen storage properties of a new Ti-V-Cr-Zr-Nb high entropy alloy // *Hydro*. 2022, v. 3, p. 270-284.

49. R. Floriano, G. Zepon, K. Edalati, G.L.B.G. Fontana, A. Mohammadi, Z. Ma, H.-W. Li, R.J. Contieri. Hydrogen storage in TiZrNbFeNi high entropy alloys, designed by thermodynamic calculations // *Int. J. Hydrogen Energy*. 2020, v. 45, p. 33759-33770.

50. R. Li, L. Xie, W.Y. Wang, P.K. Liaw, Y. Zhang. High-throughput calculations for high-entropy alloys: a brief review // *Front. Mater*. 2020, v. 7, article 290.

51. H.Y. Zhou, X.X. Lan, Z.M. Wang, Q.R. Yao, C.Y. Ni, W.P. Liu. Effect of rapid solidification on phase structure and hydrogen storage properties of $Mg_{70}(Ni_{0.75}La_{0.25})_{30}$ alloy // *Int. J. Hydrog. Energy*. 2012, v. 37, p. 13178-13184.

52. T.P. Yadav, R.M. Yadav, D.P. Singh. Mechanical milling: a top down approach for the synthesis of nanomaterials and nanocomposites // *Nanosci. Nanotechnol*. 2012, v. 2, p. 22-48.

53. S. Ranganathan. Alloyed pleasures: multi-metallic cocktails // *Curr. Sci India*. 2003, v. 85(10), p. 1404-1406.

54. C.Y. Cheng, Y.C. Yang, Y.Z. Zhong, Y.Y. Chen, T. Hsu, J.W. Yeh. Physical metallurgy of concentrated solid solutions from low-entropy to high-entropy alloys // *Curr. Opin. Solid St. Mater*. 2017, v. 21(6), p. 299-311.

55. Z. Wu, F.S. Yang, Z.W. Bao, S.N. Nyamsi, Y.Q. Wang, Z.X. Zhang. Microstructure and improved hydrogen storage properties of Mg based alloy powders prepared by modified milling method // *Powder Metall*. 2014, v. 57(1), p. 45-53.

56. Z. Wu, Z.X. Zhang, F.S. Yang, P.H. Feng, Y.Q. Wang. Hydrogen storage properties and mechanisms of magnesium based alloys with mesoporous surface // *Int. J. Hydrogen Energy*. 2016, v. 41, p. 2771-2780.

57. K.R. Cardoso, V. Roche, A.M. Jorge Jr, F.J. Antiqueira, G. Zepon, Y. Champion. Hydrogen storage in MgAlTiFeNi high entropy alloy // *J. Alloy Compd*. 2021, v. 858, p. 158357.

58. J. Montero, G. Ek, M. Sahlberg, C. Zlotea. Improving the hydrogen cycling properties by Mg addition in Ti-V-Zr-Nb refractory high entropy alloy // *Scripta Mater*. 2021, v. 194, p. 1359-6462.

59. M.O. de Marco, Y. Li, H.W. Li, K. Edalati, R. Floriano. Mechanical synthesis and hydrogen storage characterization of MgVCr and MgVTiCrFe high-entropy alloy // *Adv. Eng. Mater*. 2020, v. 22, p. 1901079.

60. S.K. Dewangan, V.K. Sharma, P. Sahu, V. Kumar. Synthesis and characterization of hydrogenated novel AlCrFeMnNiW high entropy alloy // *Int. J. Hydrogen Energy*. 2020, v. 45, p. 16984-16991.

61. R.B. Strozi, D.R. Leiva, J. Huot, W.J. Botta, G. Zepon. Synthesis and hydrogen storage behavior of Mg-V-Al-Cr-Ni high entropy alloys // *Int. J. Hydrogen Energy*. 2021, v. 46, p. 2351-2361.

62. D.B. Miracle and O.N. Senkov. A critical review of high entropy alloys and related concepts // *Acta Mater*. 2017, v. 122, p. 448-511.

63. L. Luo, L. Chen, L. Li, S. Liu, Y. Li, C. Li, L. Li, J. Cui, Y. Li. High-entropy alloys for solid hydrogen storage: a review // *Int. J. Hydrogen Energy*. 2024, v. 50, p. 406-430.

64. I. Kunce, M. Polan´ski, and T. Czujko. Micro-structures and hydrogen storage properties of LaNiFeVMn alloys // *Int. J. Hydrogen Energy*. 2017, v. 42, p. 27154-27164.

65. G. Zepon, D.R. Leiva, R.B. Strozi, A. Bedoch, S.J.A. Figueroa, T.T. Ishikawa, and W.J. Botta. Hydrogen-induced phase transition of $MgZrTiFe_{0.5}Co_{0.5}Ni_{0.5}$ high entropy alloy // *Int. J. Hydrogen Energy*. 2018, v. 43(3), p. 1702-1708.

66. M.M. Nygård, G. Ek, D. Karlsson, M. Sahlberg, M.H. Sørby, and B.C. Hauback. Hydrogen storage in high-entropy alloys with varying degree of local lattice strain // *Int. J. Hydrogen Energy*. 2019, v. 44, p. 29140-29149.

67. R.B. Strozi, D.R. Leiva, J. Huot, W.J. Botta, and G. Zepon. Synthesis and hydrogen storage behavior of Mg-V-Al-Cr-Ni high entropy alloys // *Int. J. Hydrogen Energy*. 2020, v. 46, p. 2351-2361.

68. Y. Zhang, Y.J. Zhou, J.P. Lin, G.L. Chen, P.K. Liaw. Solid-solution phase formation rules for multi-component alloys // *Adv. Eng. Mater*. 2008, v. 10(6), p. 534-538.

69. S. Guo, C. Ng, J. Lu, C.T. Liu. Effect of valence electron concentration on stability of fcc or bcc phase in high entropy alloys // *J. Appl. Phys*. 2011, v. 109, article 103505.

70. X. Yang, Y. Zhang. Prediction of high-entropy stabilized solid-solution in multi-component alloys // *Mater. Chem. Phys*. 2012, v. 132(2-3), p. 233-238.

71. Z. Wu, F. Yang, Z. Bao, S. Nyallang, Z. Zhang. Improvement in hydrogen storage characteristics of Mg-based metal hydrides by doping nonmetals with high electronegativity: a first-principle study // *Comput. Mater. Sci*. 2013, v. 78, p. 83-90.

72. Z. Lu, J. Wang, Y. Wu, X. Guo, W. Xiao, Predicting hydrogen storage capacity of V-Ti-Cr-Fe alloy via ensemble machine learning // *Int. J. Hydrog. Energy*. 2022, v. 47, p. 34583-34593.

73. M.M. Nygård, G. Ek, D. Karlsson, M.H. Sorby, M. Sahlberg, and B.C. Hauback. Counting electrons - a new approach to tailor the hydrogen sorption properties of high-entropy alloys // *Acta Mater*. 2019, v. 175, p. 121-129.

74. A. Keith, C. Zlotea, P.Á. Szilágyi. Perspective of interstitial hydrides of high-entropy alloys for vehicular hydrogen storage // *Int. J. Hydrogen Energy*. 2024, v. 52, p. 531-546.

75. T.R. Somo, M.V. Lototskyy, V.A. Yartys, M.W. Davids, S.N. Nyamsi. Hydrogen storage behaviours of high entropy alloys: A Review // *J. Energy Storage*. 2023, v. 73, p. 108969.

76. R. Floriano, G. Zepon, K. Edalati, G.L.B. Fontana, A. Mohammadi, Z. Ma, H.-W. Li, R.J. Contieri. Hydrogen storage properties of new A_3B_2-type TiZrNbCrFe high-entropy alloy // *Int. J. Hydrogen Energy*. 2021, v. 46, p. 23757-23766.

77. R.B. Strozi, B.H. Silva, D.R. Leiva, C. Zlotea, W. Botta, G. Zepon. Tuning the hydrogen storage properties of Ti-V-Nb-Cr alloys by controlling the Cr/(TiVNb) ratio // *J. Alloys Compd*. 2022, v. 932, p. 167609.

78. B. Cheng, Y. Li, X. Li, H. Ke, L. Wang, T. Cao, D. Wan, B. Wang, Y. Xue. Solid-state hydrogen storage properties of Ti-V-Nb-Cr high-entropy alloys and the associated effects of transitional metals (M = Mn, Fe, Ni) // *Acta Metall. Sin. (Engl. Lett.).* 2023, v. 36, p. 1113-1122.

79. N. Otani, A. Kuwabara, T. Ogawa, C.A.J. Fisher, I. Tanaka, E. Akiba. Equilibrium hydrogen pressures in the V-H system from first principles // *Int. J. Hydrogen Energy*. 2019, v. 44, p. 28909-28918.

80. M. Rkhis, A. Alaoui-Belghiti, S. Laasri, S. Touhtouh, A. Hajjaji, E.K. Hlil, L. Bessais, D. Soubane, K. Zaidat, and S. Obbade. First principle investigation on hydrogen solid storage in $Zr_{1-x}Nb_xNiH_3$ (x=0 and 0.1) // *Int. J. Hydrogen Energy*. 2019, v. 44, p. 23188-23195.

81. N. Bourgeois, J.C. Crivello, P. Cenedese, and J.M. Joubert. Systematic first-principles study of binary metal hydrides // *ACS Comb. Sci*. 2017, v. 19, p. 513-523.

82. Y. Bouhadda, A. Rabehi, Y. Boudouma, N. Fenineche, S. Drablia, and H. Meradji. Hydrogen solid storage: First-principles study of $ZrNiH_3$ // *Int. J. Hydrogen Energy*. 2009, v. 34, p. 4997-5002.

83. J. Hu, H. Shen, M. Jiang, H. Gong, H. Xiao, Z. Liu, G. Sun, X. Zu. A DFT study of hydrogen storage in high-entropy alloy TiZrHfScMo // *Nanomater*. 2019, v. 9(3), p. 461.

84. J. Hu, J. Zhang, H. Xiao, L. Xie, G. Sun, H. Shen, P. Li, J. Zhang, X. Zu. A first-principles study of hydrogen storage of high entropy alloy TiZrVMoNb // *Int. J. Hydrogen Energy*. 2021, v. 46(40), p. 21050-21058.

85. M. Witman, S. Ling, D.M. Grant, G.S. Walker, S. Agarwal, V. Stavila, M.D. Allendorf. Extracting an empirical intermetallic hydride design principle from limited data via interpretable machine learning // *J. Phys. Chem. Lett.* 2020, v. 11, p. 40-47.

86. S. Suwarno, G. Dicky, A. Suyuthi, M. Effendi, W. Witantyo, L. Noerochim, M. Ismail. Machine learning analysis of alloying element effects on hydrogen storage properties of AB_2 metal hydrides // *Int. J. Hydrogen Energy*. 2022, v. 47, p. 11938-11947.

87. Z. Lu, J. Wang, Y. Wu, X. Guo, W. Xiao. Predicting hydrogen storage capacity of V-Ti-Cr-Fe alloy via ensemble machine learning // *Int. J. Hydrogen Energy*. 2022, v. 47, p. 34583-34593.

88. A. Verma, N. Wilson, K. Joshi. Solid state hydrogen storage: Decoding the path through machine learning // *Int. J. Hydrogen Energy*. 2024, v. 50, p. 1518-1528.

89. M. Sahlberg, D. Karlsson, C. Zlotea, U. Jansson. Superior hydrogen storage in high entropy alloys // *Sci. Rep*. 2016, v. 6, p. 36770.

90. C. Zlotea, M.A. Sow, G. Ek, J.P. Couzinié, L. Perrière, I. Guillot, J. Bourgon, K.T. Møller, T.R. Jensen, E. Akiba, M. Sahlberg. Hydrogen sorption in TiZrNbHfTa high entropy alloy // *J. Alloys Compd*. 2019, v. 775, p. 667-674.

91. R.B. Strozi, D.R. Leiva, J. Huot, W. Botta, G. Zepon. An approach to design single BCC Mg-containing high entropy alloys for hydrogen storage applications // *Int. J. Hydrogen Energy*. 2021, v. 46(50), p. 25555-25561.

92. D. Karlsson, G. Ek, J. Cedervall, C. Zlotea, K.T. Møller, T.C. Hansen, J. Bednarčík, M. Paskevicius, M.H. Sørby, T.R. Jensen, U. Jansson, and M. Sahlberg. Structure and hydrogenation properties of a HfNbTiVZr high-entropy alloy // *Inorg. Chem*. 2018, v. 57, p, 2103-2110.

93. J. Hu, J. Zhang, H. Xiao, L. Xie, H. Shen, P. Li, J. Zhang, H. Gong, and X. Zu. A density functional theory study of the hydrogen absorption in high entropy alloy TiZrHfMoNb // *Inorg. Chem*. 2020, v. 59, p. 9774-9782.

94. B.H. Silva, C. Zlotea, Y. Champion, W.J. Botta, and G. Zepon. Design of TiVNb-(Cr, Ni or Co) multicomponent alloys with the same valence electron concentration for hydrogen storage // *J. Alloys Compd*. 2021, v. 865, p. 158767.

95. S. Sleiman, J. Huot. Effect of particle size, pressure and temperature on the activation process of

hydrogen absorption in TiVZrHfNb high entropy alloy // *J. Alloys Compd*. 2021, v. 861, p. 158615.

96. H. Hu, C. Ma, and Q. Chen. Mechanism and microstructural evolution of TiCrVFe hydrogen storage alloys upon de-/hydrogenation // *J. Alloys Compd*. 2021, v. 877, p. 160315.

97. C. Zhang, A. Song, Y. Yuan, Y. Wu, P. Zhang, Z. Lu, X. Song. Study on the hydrogen storage properties of a TiZrNbTa high entropy alloy // *Int. J. Hydrogen Energy*. 2020, v. 45, p. 5367-5374.

98. S. Yang, F. Yang, C. Wu, Y. Chen, Y. Mao, and L. Luo. Hydrogen storage and cyclic properties of $(VFe)_{60}(TiCrCo)_{40-x}Zr_x$ $(0 \le x \le 2)$ alloys // *J. Alloys Compd*. 2016, v. 663, p. 460-465.

99. J. Montero, G. Ek, L. Laversenne, V. Nassif, M. Sahlberg, C. Zlotea. How 10 at.% Al addition in the Ti-V-Zr-Nb high-entropy alloy changes hydrogen sorption properties // *Molecules*. 2021, v. 26, p. 2470.

100. L. Serrano, M. Moussa, J.Y. Yao, G. Silva, J.L. Bobet, S.F. Santos, K.R. Cardoso. Development of Ti-V-Nb-Cr-Mn high entropy alloys for hydrogen storage // *J. Alloy Compd*. 2023, v. 945, p. 169289.

101. I. Kunce, M. Polanski, J. Bystrzycki. Structure and hydrogen properties of a high entropy ZrTiVCrFeNi alloy synthesized using Laser Engineered Net Shaping (LENS) // *Int. J. Hydrogen Energy*. 2013, v. 38, p. 12180-12189.

102. J. Chen, Z. Li, H. Huang, Y. Lv, B. Liu, Y. Li, Y. Wu, J. Yuan, Y. Wang. Superior cycle life of TiZrFeMnCrV high entropy alloy for hydrogen storage // *Scripta Mater*. 2022, v. 212, p. 114548.

103. R. Floriano, G. Zepon, K. Edalati, G.L.B. Fontana, A. Mohammadi, Z. Ma, H.-W. Li, R.J. Contieri. Hydrogen storage in TiZrNbFeNi high entropy alloys, designed by thermodynamic calculations // *Int. J. Hydrogen Energy*. 2020, v. 45, p. 33759-33770.

104. R. Floriano, G. Zepon, K. Edalati, G.L.B. Fontana, A. Mohammadi, Z. Ma, H.-W. Li, R.J. Contieri. Hydrogen storage properties of new A_3B_2-type TiZrNbCrFe high-entropy alloy // *Int. J. Hydrogen Energy*. 2021, v. 46, p. 23757-23766.

105. G. Andrade, G. Zepon, K. Edalati, A. Mohammadi, Z. Ma, H.-W. Li, R. Floriano. Crystal structure and hydrogen storage properties of AB-type TiZrNbCrFeNi high-entropy alloy // *Int. J. Hydrogen Energy*. 2023, v. 48, p. 13555-13565.

106. K.-F. Yao, H.-W. Luan, Y. Shao, J.-F. Li, W.-L. Mao, Z.-D. Han, C. Shao. Phase stabilities of high entropy alloys // *Scripta Mater*. 2020, v. 179, p. 40-44.

107. M. Lototskyy, V.A. Yartys. Comparative analysis of the efficiencies of hydrogen storage systems utilising solid state H storage materials // *J. Alloy. Compd*. 2015, v. 645, p. S365-S373.

108. S. Dangwal, K. Edalati. Significance of interphase boundaries on activation of high-entropy alloys for room-temperature hydrogen storage // *Int. J. Hydrogen Energy*. 2024, v. 50, p. 626-636.

109. S. Dangwal, K. Edalati. High-entropy alloy TiV2ZrCrMnFeNi for hydrogen storage at room temperature with full reversibility and good activation // *Scripta Mater*. 2024, v. 238, p. 115774.

110. F. Pineda, C. Martínez, P. Martin, C. Aguilar. High-entropy alloys: A review of their performance as promising materials for hydrogen and molten salt storage // *Rev. Adv. Mater. Sci*. 2023, v. 62(1), p. 20230150.

111. A. Kumar, T. Prasad, N. Krishna. Notable hydrogen storage in Ti-Zr-V-Cr-Ni high entropy alloy // *Int. J. Hydrog. Energy*. 2022, v. 47, p. 22893-22900.

112. T. Fukagawa, Y. Saito, A. Matsuyama. Effect of varying Ni content on hydrogen absorption–desorption and electrochemical properties of Zr-Ti-Ni-Cr-Mn high-entropy alloys // *J. Alloys Compd*. 2022, v. 896, p. 163118.

Article received 04.04.2024

ЗАСТОСУВАННЯ ВИСОКОЕНТРОПІЙНИХ СПЛАВІВ У ТЕХНОЛОГІЯХ ЗБЕРІГАННЯ ВОДНЮ

Сергій Карпов

Високоентропійні сплави (ВЕС) – новий клас матеріалів з багатообіцяючими структурними та функціональними властивостями, останнім часом привертають значну увагу у різних галузях, включаючи зберігання водню. Їх унікальна концепція дизайну і широке композиційне різноманіття відкривають безпрецедентні можливості для розробки передових матеріалів для зберігання водню. Цей огляд має на меті систематично проаналізувати сучасний стан досліджень ВЕСів для зберігання водню, приділяючи особливу увагу композиційній побудові, процесам синтезу та характеристикам при зберіганні водню. В огляді також аналізується зв’язок між ефективністю зберігання водню і властивостями, пов'язаними зі складом, зокрема для матеріалів, що кристалізуються у вигляді ОЦК-сплавів і сплавів з фазою Лавеса. Детально розглянуто різні аспекти взаємодії водню з ВЕСами, включаючи оборотність зберігання водню, циклічну стабільність і проблеми з активацією. Підкреслено потенціал ВЕСів у розробці нових матеріалів для зберігання водню з високими характеристиками, з урахуванням подальшого удосконалення композиційної побудови та методів синтезу.